

Article

Crilin: A Semi-Homogeneous Calorimeter for a Future Muon Collider

Sergio Ceravolo ¹, Francesco Colao ², Camilla Curatolo ³, Elisa Di Meco ^{1,*}, Eleonora Diociaiuti ¹, Donatella Lucchesi ⁴, Daniele Paesani ¹, Nadia Pastrone ⁵, Gianantonio Pezzullo ⁶ , Alessandro Saputi ⁷ , Ivano Sarra ¹, Lorenzo Sestini ⁴ and Diego Tagnani ⁸

¹ Istituto Nazionale di Fisica Nucleare, Laboratori Nazionali di Frascati, Via Enrico Fermi 54, 00054 Frascati, Italy

² Enea Frascati, Via Enrico Fermi 45, 00044 Frascati, Italy

³ Istituto Nazionale di Fisica Nucleare, Sezione di Milano, Via Celoria 16, 20133 Milano, Italy

⁴ Istituto Nazionale di Fisica Nucleare, Sezione di Padova, Via Francesco Marzolo 8, 35131 Padova, Italy

⁵ Istituto Nazionale di Fisica Nucleare, Sezione di Torino, Via Pietro Giuria 1, 10125 Torino, Italy

⁶ Department of Physics, Yale University, New Heaven, CT 06511, USA

⁷ Istituto Nazionale di Fisica Nucleare, Sezione di Ferrara, Via Saragat 11, 44122 Ferrara, Italy

⁸ Istituto Nazionale di Fisica Nucleare, Sezione di Roma Tre, Via della Vasca Navale 84, 00146 Roma, Italy

* Correspondence: elisa.dimeco@lnf.infn.it



Citation: Ceravolo, S.; Colao, F.; Curatolo, C.; Di Meco, E.; Diociaiuti, E.; Lucchesi, D.; Paesani, D.; Pastrone, N.; Pezzullo, G.; Saputi, A.; et al.

Crilin: A Semi-Homogeneous Calorimeter for a Future Muon Collider. *Instruments* **2022**, *6*, 62. <https://doi.org/10.3390/instruments6040062>

Academic Editors: Fabrizio Salvatore, Alessandro Cerri, Antonella De Santo and Iacopo Vivarelli

Received: 16 September 2022

Accepted: 8 October 2022

Published: 11 October 2022

Publisher's Note: MDPI stays neutral with regard to jurisdictional claims in published maps and institutional affiliations.



Copyright: © 2022 by the authors. Licensee MDPI, Basel, Switzerland. This article is an open access article distributed under the terms and conditions of the Creative Commons Attribution (CC BY) license (<https://creativecommons.org/licenses/by/4.0/>).

Abstract: Calorimeters, as other detectors, have to face the increasing performance demands of the new energy frontier experiments. For a future Muon Collider the main challenge is given by the Beam Induced Background that may pose limitations to the physics performance. However, it is possible to reduce the BIB impact by exploiting some of its characteristics by ensuring high granularity, excellent timing, longitudinal segmentation and good energy resolution. The proposed design, the Crilin calorimeter, is an alternative semi-homogeneous ECAL barrel for the Muon Collider based on Lead Fluoride Crystals (PbF₂) with a surface-mount UV-extended Silicon Photomultipliers (SiPMs) readout with an optimized design for a future Muon Collider.

Keywords: calorimeters; PbF₂; SiPM; crystals; high granularity

1. Introduction

The idea of developing a Muon Collider facility was born as an alternative to electron and hadron accelerators with the aim to reach the Multi-TeV range and unlock new discoveries. This choice would have unique advantages, since clean events as in electron-positron colliders are possible, and high collision energy as in hadron colliders could be reached due to negligible beam radiation losses.

Unfortunately the expected environment is not truly clean because of the presence of the beam-induced background (BIB), produced by the decay of Muons and subsequent interactions with the machine elements. This might reduce the physics performance, however it is possible to reduce the effect of the BIB resolution degradation by exploiting some characteristics. The BIB arrival hit arrival time is expected to be out-of-time with respect to the bunch crossing. In addition, the longitudinal energy distribution of the BIB particles will be different from particles from the primary interaction which are expected to propagate deeper into the detector. Another one is the longitudinal energy deposit distribution of the BIB particles that is expected to be deposited in the innermost layers of the calorimeter, while particles coming from the primary interaction propagate deeper in the detector. The technology and the design of the calorimeters should be chosen to reduce the effect of the BIB, while keeping good physics performance. This can be achieved with four main requirements:

- High granularity to reduce the overlap of BIB particles in the same calorimeter cell.

- Good timing resolution can be utilised to reduce the out-of-time component of the BIB (Figure 1-left). A time resolution of about $\sigma_t = 80$ ps should be achieved.
- Longitudinal segmentation since the signal energy profile in the longitudinal direction is different from the BIB one, hence a segmentation of the calorimeter can help distinguishing the signal showers from the fake showers produced by the BIB (Figure 1-right).
- Good energy resolution, $10\%/\sqrt{E}$ in the ECAL system is expected to be enough to obtain good physics performance.

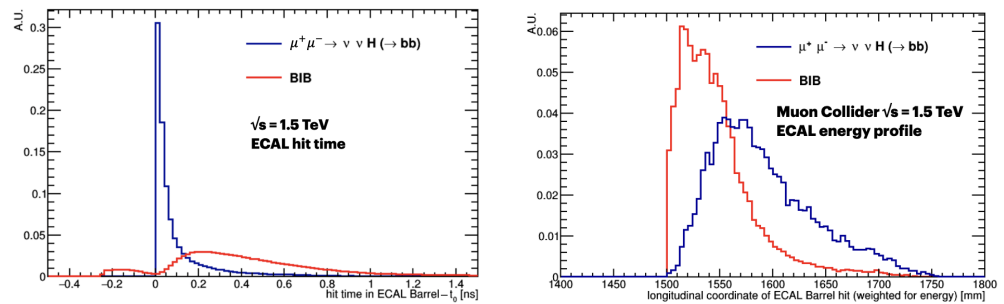


Figure 1. The (left) panel shows the time of the ECAL barrel hits with respect to bunch crossing time, for BIB and $H \rightarrow \bar{b}b$ signal. In the (right) one the energy distribution of ECAL barrel hits as a function of the distance with respect to the beam axis is presented [1].

The design described in the following pages is an alternative electromagnetic calorimeter for the Muon Collider: Crilin, a crystal calorimeter with longitudinal information. Crilin has a modular architecture made of stackable and interchangeable sub-modules composed of matrices of Lead Fluoride (PbF_2) crystals, where each crystal is individually readout by 2 series of 2 UV-extended surface mount Silicon Photomultipliers (SiPMs) each and represents a valid and cheaper alternative to the baseline W-Si Muon Collider ECAL barrel.

2. The Crilin Calorimeter

Crilin is a semi-homogeneous calorimeter made of sub-modules of PbF_2 crystals matrices. Each of these crystals is individually readout by two series of two UV-extended surface mounted Silicon Photomultipliers (SiPMs). The essential advantages of this choice consist in an excellent compromise of the following features:

- As the Cherenkov light production in PbF_2 is instantaneous with respect to the particle passage this leads to an inherently fast detector response and excellent timing resolution.
- Narrow signals hence an excellent ability to temporally resolve close events at high rate.
- A good light collection that enables a fine energy resolution throughout the whole dynamic range.
- Resistance to radiation.
- Fine granularity that scales with the SiPMs dimensions.

All these advantages are combined with a substantial reduction of the costs compared to other technologies, together with longitudinal segmentation and excellent time resolution. The Crilin ECAL barrel design for the Muon Collider, simulated in Figure 2, consists of five layers with 40 mm thick, and 10×10 mm² of cell area PbF_2 crystals provided by SICCAS readout with a matrix (2×2) of 4 Hamamatsu SiPMs per crystal.

In order to demonstrate the viability of the Crilin technology, the simulation framework of the International Muon Collider Collaboration has been employed. With this purpose the W-Si ECAL barrel used in this simulation framework has been substituted with the Crilin calorimeter and the performances have been compared. This was carried out on objects of primary interest for Muon Collider physics: hadronic jets.

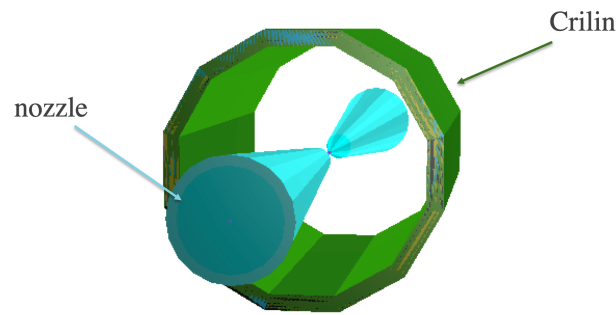


Figure 2. Geant4 realisation of Crilin using a dodecahedra geometry together with nozzles.

A Particle Flow algorithm [2], not yet fully optimized, was employed for jet reconstruction. The full simulation of b -jets has been used for this purpose, and the beam-induced background as been simulated as well. The jet reconstruction efficiency and jet p_T resolutions are presented in Figure 3. It can be noticed that the performance is similar in the two cases but, at the same time, the money cost of Crilin is a factor 10 less.

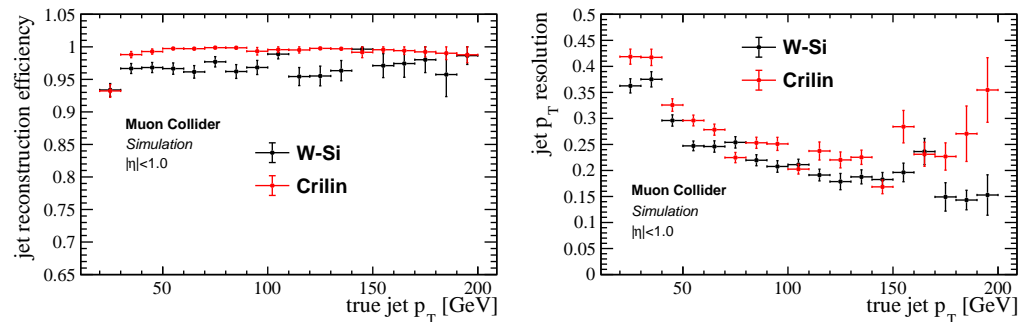


Figure 3. (Left): jet reconstruction efficiency as a function of the jet p_T , obtained by using the Crilin ECAL barrel and the W-Si ECAL barrel. (Right): jet p_T resolution as a function of the jet p_T , obtained by using the Crilin ECAL barrel and the W-Si ECAL barrel.

Radiation Hardness and Crystals Characterisation

As anticipated the beam induced background represents a real challenge for the Muon Collider detectors not only from the point of view of resolution performances but also in terms of radiation hardness. This is why the BIB at $\sqrt{s} = 1.5$ TeV has been simulated by means of FLUKA on a simplified collider geometry. The dose maps are available in Figure 4 where both of them are normalised to one year of operation (200 days/year) for a 2.5 km circumference ring with 5 Hz injection frequency. The 1-MeV-neq fluence is expected to be $\sim 10^{14} \text{ cm}^{-2} \text{ y}^{-1}$ in the electromagnetic calorimeter, with a steeply decreasing radial dependence beyond it. The total ionizing dose is instead $\sim 10^{-4}$ Grad/y on the electromagnetic calorimeter.

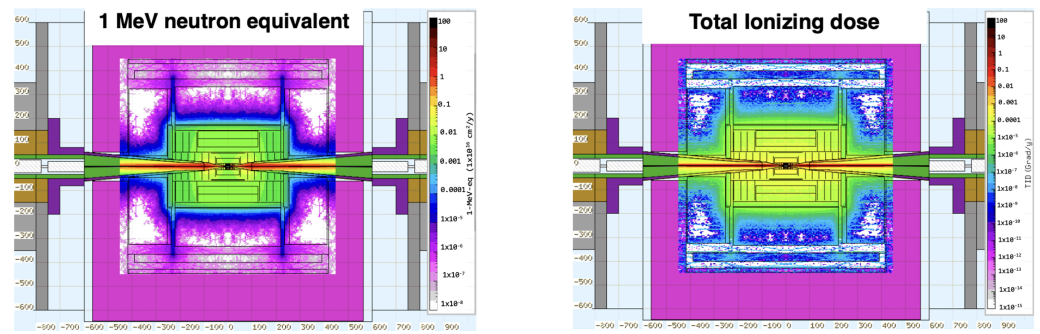


Figure 4. (Left): Map of the 1-MeV-neq fluence in the detector region for a Muon Collider operating at $\sqrt{s} = 1.5$ TeV with the parameters described in [3], shown as a function of the position along the beam axis and the radius. (Right): Map of the TID in the detector region shown as a function of the position along the beam axis and the radius.

Once the BIB effects were predicted it was necessary to evaluate the consequent deterioration of the single components of the Crilin ECAL, starting with a crystal characterization campaign. The aim was to compare the transmittance spectrum of two PbF_2 crystals. They were sized $5 \times 5 \times 40 \text{ mm}^3$ and manufactured by SICCAS using a melt growth process, thus resulting in a cubic form ($\beta\text{-PbF}_2$). Measurements were performed with and without a Mylar wrapping, before and after irradiation with both photons and neutrons. The photon irradiation phase was carried out at ENEA-Calliope, a pool-type gamma irradiation facility equipped with a ^{60}Co radio-isotopic source array producing photons with $E_\gamma = 1.25 \text{ MeV}$. The two crystals were exposed to different irradiation steps during three days and in Figure 5 it is possible to observe the longitudinal transmittance spectra obtained for the two crystals. After a TID of approximately 80 krad, close to the Muon Collider expected one, no significant decrease in transmittance was observed. It is worth noticing that after this dose a saturation effect associated with the damage mechanism is shown, as already observed in [4], and that the maximum degradation is at the level of 40% [5].

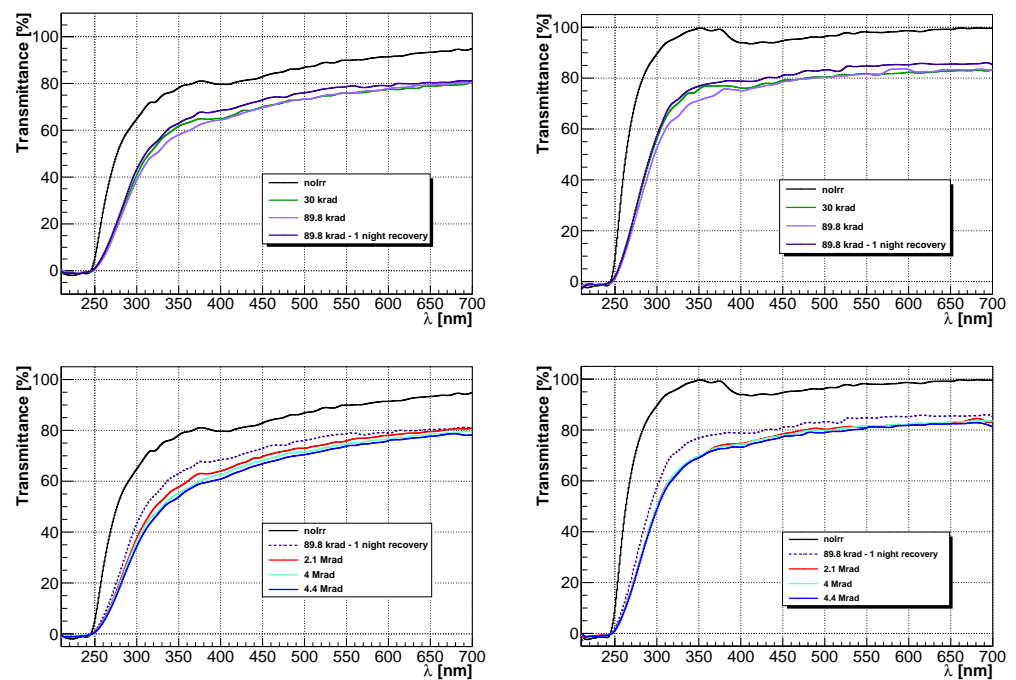


Figure 5. Transmission spectra obtained in the different irradiation steps for the naked crystal (top and bottom left) and the crystal with Mylar wrapping (top and bottom right).

The second characterization has been carried out with neutron irradiation at the the ENEA Frascati Neutron Generator facility, based on the $T(d,n)\alpha$ fusion reaction. The source provided 14 MeV neutrons with a total fluence of 10^{13} n/cm² for a total amount of time of one hour and 30 min. However, because of some technical time related to logistics and shipment of the crystals, transmittance measurements could only be performed 14 days after the irradiation and showed no alteration in the transmittance spectrum as reported in Figure 6. This result indeed highlights the natural annealing of these crystals.

A neutron irradiation campaign has been very recently carried out also for the SiPMs in order to test the radiation hardness of two different pixel dimension Hamamatsu SMD sensors choices (10 μ and 15 μ) however the analysis is still ongoing.

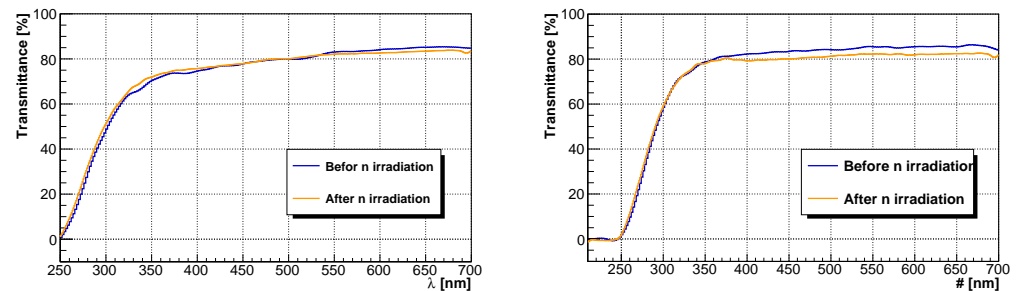


Figure 6. Transmission spectra obtained after the irradiation at FNG with 14 MeV neutrons for a total fluence of 10^{13} n/cm² (orange line) compared with the results after the 16 hours optical bleaching (blue line) for the naked crystal (left) and for the crystal with Mylar wrapping (right).

3. The Crilin Prototype

The full prototype design of the Crilin ECAL for the Muon Collider will consist of four layers of 5×5 PbF₂ crystals each readout by thin SMD SiPMs by Hamamatsu. And will operate at a temperature of 0/−10 °C. A one layer 2 crystals preliminary prototype (Proto-0) has already been built in 2021 and tested at Beam Test Facility of Laboratori Nazionali of Frascati with 500 MeV electrons in July 2021 and at H2 test facility of CERN with 120 GeV electrons in August 2021. The ongoing analysis is already showing promising results both in terms of time resolution (less than 100 ps for deposit energies greater than 1 GeV) and energy resolution (1 p.e./MeV of light yield) however further improvements of these results can be achieved. Is now under construction a larger and improved prototype, Proto-1, made of two sub-modules, each composed of a 3×3 crystals matrix and with a new choice of SMD sensors, the Hamamatsu S14160-3015PS [6] ones. A rendering of Proto-1 is represented in Figure 7 together with a close up look at the single module (on the right). The SiPMs have already been tested with the new front end electronics and results will be shown in the following pages.

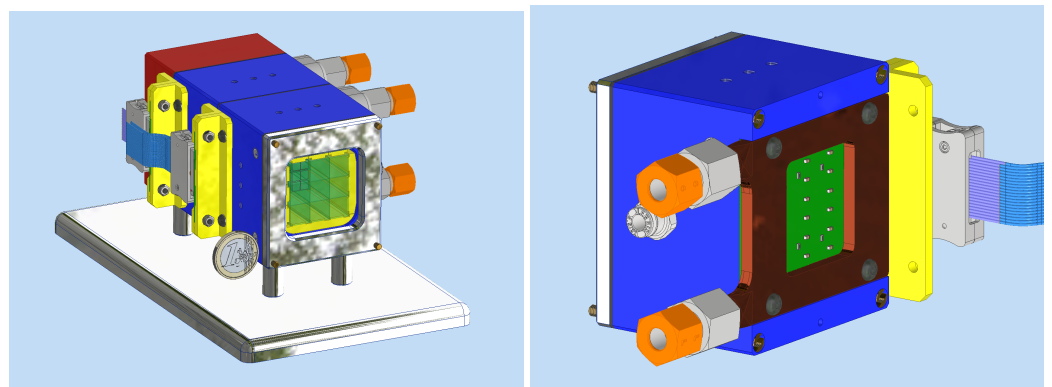


Figure 7. CAD 3D model of Crilin Prototype (Proto-1) on the (left). On the (right) a single module detail showing the cold plate heat exchanger mounted over the electronic board.

Thanks to the tests and analysis performed on Proto-0 it was possible to set some requirements in order to improve the electronic system. The new front end electronics is now made of two distinct parts: the SiPM boards and the Mezzanine boards. Each SiPM board, in Figure 8-left, is made of 36 photo-sensors so that each crystal in the matrix has two separate and independent readout channels, consisting in a series of two 15 μm pixel-size SMD S14160-3015PS SiPMs. These were chosen for their high-speed response, narrow signals and radiation hardness. Four 0603 SMD blue LEDs were also placed in between the SiPMs matrices in order to perform in-situ calibration, diagnostic and monitoring. The SiPMs are then connected via 50 Ω micro-coaxial transmission lines to a microprocessor-controlled Mezzanine Board (right panel in Figure 8).

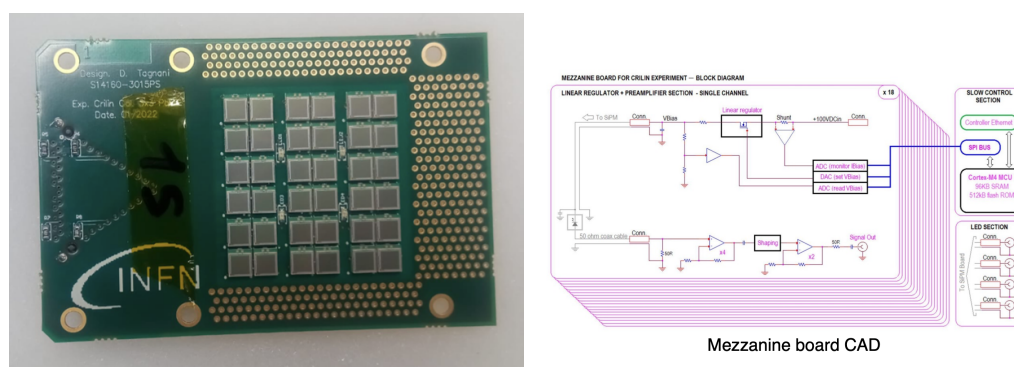


Figure 8. (Left): SiPMs board detail, showing the sensor matrices and the LEDs. (Right): Mezzanine Boards CAD rendering.

The Mezzanine Board provides signal amplification and shaping, along with all slow control functions for all the 18 readout channels. Signals are shaped and amplified by means of two non inverting amplification stages and a pole-zero cancellation network with a dynamic range of 2 V and an overall gain of 8. The SiPMs biasing is controlled by 12-bit DACs while regulated voltages, bias currents, and the temperature of the SiPM matrix are sensed via dedicated 12-bit ADC channels. The slow control routines are then handled by an onboard Cortex M4 microprocessor.

The prototype consists of two sub-modules, each composed of a 3 \times 3 crystals matrix and arranged in a series and assembled by bolting, leading to a compact and small calorimeter (Figure 7-left). The operational temperature for this prototype is going to be 0 $^{\circ}\text{C}$. Since the total heat load has been estimated to be 350 mW per crystals (per two channels) a cooling system was necessary. This system consists of a cooling plant and a cold plate heat exchanger in direct contact with the electronic board. A cold plate heat exchanger, made of copper, is mounted over the electronic board and a glycol based water solution, supplied by the cooling plant, passes through the deep drilled channels to absorb the SiPMs generated heat (Figure 7-right).

FEE and SiPMs Tests

A first prototype of the front-end electronics was tested by exposing two 15 μm SiPMs to a picosecond UV laser source while signals were digitised using a 40 GS/s oscilloscope. The aim was to evaluate the time resolution performances by reconstructing timing using a log-normal fit applied to SiPM pulse rising edge and a constant fraction technique. A digitised waveform is presented in Figure 9-left. The time resolution was evaluated in three different situations:

1. Constant laser pulse amplitude (adjusted in order to have signals with 1 V peak amplitude) and fixed 40 Gps sample rate, while laser repetition rate was increased from 50 kHz up to 5 MHz.
2. Fixed laser amplitude (as before) and fixed 100 kHz laser repetition rate, while the oscilloscope sample rate was swept in the range 2.5 to 40 Gps.

- Fixed laser repetition rate and sampling frequency, while the waveform peak amplitude was swept over the FEE dynamic range.

The first measurements the waveform peak amplitude and the sampling rate were set to 1 V and 40 Gsps. Figure 9-right actually shows that the waveform profiles remained unchanged throughout the test and no effect on the timing resolution was found for laser repetition rates in the range 50 kHz–5 MHz.

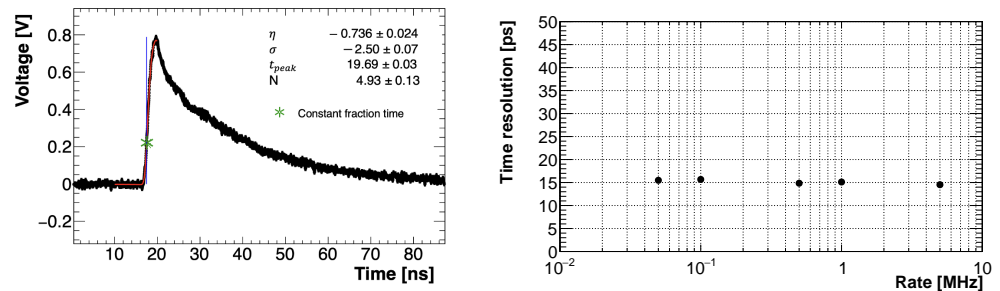


Figure 9. (Left): SiPM waveform in response to a laser pulse, sampled at 40 GS/s. Log-normal fit on the rising edge is overlaid. (Right): Effect of laser repetition rate on the time resolution.

The second dataset was carried out by changing the oscilloscope sample rate in the range 2.5 Gsps–40 Gsps while the waveform peak amplitude and the laser repetition rate were fixed at 1 V and 100 kHz. The effect of the sampling rate is summarised in Figure 10-left, which shows the strong dependence of the time resolution from the digitizer sample rate since it scales from the worst-case $\sigma_t \sim 32$ ps obtained at 2.5 GS/s to $\sigma_t \sim 15$ ps at 40 GS/s.

The charge dependence of the time resolution was evaluated with a dedicated set of measurements carried out at 40 GS/s, using fixed laser repetition rate of 100 kHz, and six different laser amplitude settings. Pulse charges were evaluated by integrating each waveform taking into account the 50Ω oscilloscope input impedance. For each of the six runs the charge distribution was Gaussian therefore the reference value was evaluated as the mean value of a normal fit. Taking into account the SiPMs and FEE gains it was possible to convert the charge value to the corresponding number of photo-electrons $N_{p.e.}$, thus resulting in a conversion factor of ~ 2.48 photo-electrons per pC. The time resolution dependence on charge and $N_{p.e.}$ was then evaluated in (Figure 10-right).

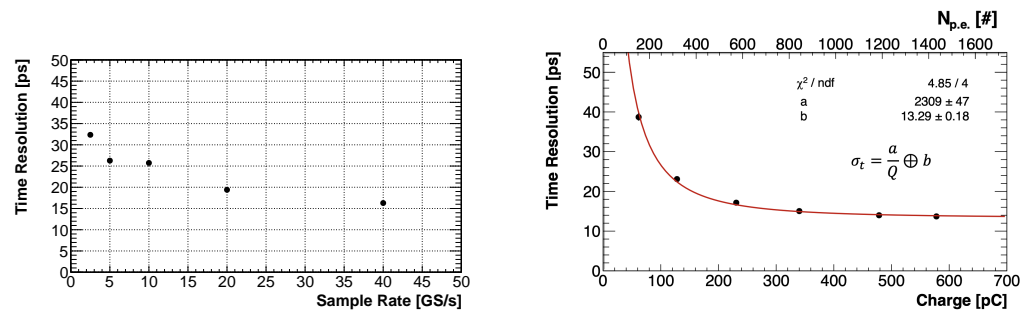


Figure 10. Effect of sampling frequency on time resolution (left). Time resolution as a function of charge and $N_{p.e.}$ (right).

This last scan points up the high performances that the calorimeter electronics can reach by showing a time resolution that is already less than 40 ps even at low charges (50 pC–124 photo-electrons) and an impressive constant term b of ~ 13 ps.

4. Conclusions

High intensity experiments need high performance detectors capable of supporting innovative reconstruction techniques, enabling superior signal extraction from harsh and high-rate backgrounds. The described solution represents a valid and cheaper alternative to

the baseline W-Si ECAL barrel of the Muon Collider ensuring, through a semi-homogeneous calorimeter, longitudinal segmentation and a great timing resolution while enabling superior event reconstruction strategies, thanks to the use of 5D discrimination.

Single components were already characterised by estimating the radiation damages on crystals and SiPMs through irradiation studies but also with a preliminary two crystal prototype test beam carried out at BTF with 500 MeV in July 2021 and at CERN in August 2021.

Crilin Proto-1, made of 2 layers of 3×3 PbF₂ crystals will be shortly assembled. The aim is to test its performances in a new test beam at BTF with 500 MeV electrons and at H2 test facility at CERN with a high energy beam (>100 GeV) before the end of 2022 and to set new requirements for future prototypes.

Author Contributions: Writing—original draft, S.C., F.C., C.C., E.D.M., E.D., D.L., D.P., N.P., G.P., A.S., I.S., L.S. and D.T. All authors have read and agreed to the published version of the manuscript.

Funding: This research received no external funding.

Data Availability Statement: The data presented in this study are available on request from the corresponding author.

Acknowledgments: This work was developed within the framework of the International Muon Collider Collaboration (<https://muoncollider.web.cern.ch>, accessed on 7 October 2022), where the Physics and Detector Group aims to evaluate potential detector R&D to optimize experiment design in the multi-TeV energy regime. This project has received support (funding) from the European Union's Horizon 2020 Research and Innovation program under Grant Agreement No 101004761. The authors wish to thank the LNF Division Research and SPCM departments for their technical and logistic support and are grateful to the people in Enea Casaccia and Enea FNG facilities for their extensive collaboration during the irradiation campaign of crystals and photo-sensors.

Conflicts of Interest: The authors declare no conflict of interest.

References

1. Sestini, L.; Sarra, I.; Andreetto, P.; Gianelle, A.; Lucchesi, D.; Buonincontri, L.; Zuliani, D.; Casarsa, M.; Bartosik, N.; Pastrone, N.; et al. Design a calorimeter system for the Muon Collider experiment. *PoS* **2022**, *EPS-HEP2021*, 776. [[CrossRef](#)]
2. Bartosik, N.; Krizka, K.; Griso, S.P.; Aimè, C.; Apyan, A.; Mahmoud, M.A.; Bertolin, A.; Braghieri, A.; Buonincontri, L.; Calzaferri, S.; et al. Simulated Detector Performance at the Muon Collider. *arXiv* **2022**, arXiv:2203.07964. [[CrossRef](#)]
3. Collamati, F.; Curatolo, C.; Lucchesi, D.; Mereghetti, A.; Mokhov, N.; Palmer, M.; Sala, P. Advanced assessment of beam-induced background at a muon collider. *J. Instrum.* **2021**, *16*, P11009. [[CrossRef](#)]
4. Zhu, R.; Ma, D.; Newman, H.; Woody, C.; Kierstead, J.; Stoll, S.; Levy, P. A study on the properties of lead tungstate crystals. *Nucl. Instrum. Methods Phys. Res. Sect. A Accel. Spectrometers Detect. Assoc. Equip.* **1996**, *376*, 319–334. [[CrossRef](#)]
5. Cemmi, A.; Colangeli, A.; D'orsi, B.; Sarcina, I.D.; Diociaiuti, E.; Fiore, S.; Paesani, D.; Pillon, M.; Saputi, A.; Sarra, I.; et al. Radiation study of Lead Fluoride crystals. *J. Instrum.* **2022**, *17*, T05015. [[CrossRef](#)]
6. Hamamatsu SiPMs Datasheet. Available online: https://www.hamamatsu.com/content/dam/hamamatsu-photonics/sites/documents/99_SALES_LIBRARY/ssd/s14160-1310ps_etc_kapd1070e.pdf (accessed on 7 October 2022).